Angular distribution of low-energy electron emission in collisions of 6-MeV/u bare carbon ions with molecular hydrogen: Two-center mechanism and interference effect

Deepankar Misra,* A. Kelkar, U. Kadhane, Ajay Kumar, Y. P. Singh, and Lokesh C. Tribedi
Tata Institute of Fundamental Research, Homi Bhabha Road, Colaba, Mumbai 400 005, India

P. D. Fainstein
Centro Atómico Bariloche, Comisión Nacional de Energía Atómica, Avenida E. Bustillo 9500, 8400 Bariloche, Argentina
(Received 3 March 2007; published 17 May 2007)

We report the energy and angular distribution of electron double differential cross sections (DDCS) in collision of 6-MeV/u C^{6+} ions with molecular hydrogen. We explain the observed distributions in terms of the two-center effect and the Young-type interference effect. The secondary electrons having energies between 1 and 1000 eV are detected at about 10 different emission angles between 30° and 150°. The measured data are compared with the state-of-the-art continuum distorted wave-eikonal initial state and the first Born model calculations which use molecular wave function. The single differential cross sections are derived and compared with the theoretical predictions. The oscillations due to the interference effect are derived in the DDCS ratios using theoretical cross sections for the atomic H target. The effect of the atomic parameters on the observed oscillations is discussed. An evidence of interference effect has also been shown in the single differential cross section. The electron energy dependence of the forward-backward asymmetry parameter shows a monotonically increasing behavior for an atomic target, such as He, which could be explained in terms of the two-center effect only. In contrast, for the molecular H_2 the asymmetry parameter reveals an oscillatory behavior due to the Young-type interference effect superimposed with the two-center effect. The asymmetry parameter technique provides a self-normalized method to reveal the interference oscillation which does not require either a theoretical model or complementary measurements on the atomic H target.

DOI: 10.1103/PhysRevA.75.052712 PACS number(s): 34.50.Fa, 34.50.Gb

I. INTRODUCTION

The shape of the low-energy electron spectrum emitted in heavy ion atomic collisions is sensitive to the various ionization mechanisms. Spectra from double differential electron emission clearly identifies different processes, such as, soft collision electrons (SE), two-center electron emission (TCEE), electron capture to the continuum (ECC) at *zero degree* and the binary encounter (BE). Unlike the case of low charged projectiles, such as, e^-, H^+, and He^{2+}, etc., the motion of the ionized electron is considerably affected by the two moving sources of Coulomb potentials, namely, the receding highly charged heavy projectile ion and the residual recoil ion. Although, the projectile velocity considered here is much larger than the velocity of the electron in the atom, $(v_p/v_e \sim 11.5)$ it is seen that the first Born calculation (B1) fails to explain the energy and angular distributions of the ionized electrons. This is a consequence of the fact that, B1 accounts only for the target center effects and does not consider the effect of the receding projectile after the electron has been ionized. In order to account for the projectile center effects, a theoretical model based on the continuum distorted wave-eikonal initial state (CDW-EIS) approximation has been developed [1]. This method is a first order in the distorted wave series and is shown to be adequate to describe the dynamics of the ionized electron in the combined Coulomb fields of the projectile and the target. The model was extended and fine-tuned by many workers over the period of time for multielectronic targets [2].

Furthermore, the electron emission spectrum from H_2, under heavy ion impact, has revealed an additional mechanism of the Young-type interference effect affecting the shape of the DDCS spectrum. Although this effect has been observed in the case of photoionization [3,4] and electron capture [5,6], it is interesting to note that the influence of interference on the ion impact ionization of the molecule was not known until recently. It is only very recently that, the interference effect in the low-energy electron spectra emitted from H_2 has been demonstrated, in collisions with high-energy (60-MeV/u) Kr^{34+} ion impact [7] and relatively low-energy collisions [8]. The initial measurements on interference effect in ion induced ionization of H_2 has provided a lot of impetus for the revival of the study of this fundamental process in the ionization of molecules by heavy ions as well as in photoionization and electron impact ionization studies. As a result this study of Young-type interference effect has attracted a great deal of attention, both on the theoretical [9–18] as well as on the experimental fronts [19–29] and is a topic of current interest in the particle induced ionization studies. Galassi *et al.* have also extended the atomic-type CDW-EIS calculation for a diatomic molecular target such as H_2 [9] by introducing the molecular wave function. Although this model has been used to describe the interference effect in ionization of H_2, the overall energy and angular distributions of DDCSs have not yet been compared against the experimental data. Very recently, Becker and co-workers [30] have investigated the effect of isotope substitution on the interference oscillations in case of N_2 to explore the effect of two dissimilar "slits."

In this paper, we show the details of the measurements of the oscillations due to the interference in the electron DDCS

*Electronic address: dmisra@tifr.res.in, lokesh@tifr.res.in

for various forward and backward emission angles. The effect of the atomic parameter on the derived oscillations in the DDCS ratios are discussed. We also show the evidence of interference effect in the single differential cross section (SDCS) as a function of energy. In addition, we report a detailed study of two-center effect (TCE) in the collision of bare carbon ions with molecular hydrogen by measuring the energy and angular distributions of the DDCS. The hydrogen molecule has a narrower Compton profile compared to He and hence the binary peak for H_2 has less width than that for He.

The large discrepancy in the forward-backward asymmetry parameter compared to the prediction of the B1 approximation is known to be the signature of the TCE [31–35]. In addition, we show, for the H_2 target, an oscillatory structure overriding the monotonically increasing asymmetry parameter as a function of electron energy signifies the interference effect along with the TCE. This provides a method, as proposed in Ref. [28], to derive the oscillations due to interference which is self-normalized, i.e., it needs only the DDCS for the H_2, not the DDCS for atomic H. The experimental data have been compared with the modified state-of-the-art theoretical model calculations such as the CDW-EIS and the B1 approximations which use a molecular wave function [9].

II. MEASUREMENTS AND EXPERIMENTAL RESULTS

The present measurements were carried out for impact of 6 MeV/u C^{6+} ions with H_2. The BARC-TIFR Pelletron accelerator facility at Mumbai was used to obtain the ion beams. The mass analyzed C^{6+} ions were energy analyzed by a 90° analyzing magnet. The beam was collimated by two sets of 4-jaw slits (2×2 mm^2) placed 1 meter apart. Finally, the beam was cut by a 4 mm circular aperture before it entered the scattering chamber and interacted with the target atoms. The last aperture was essential to cut down the forward moving electrons which are generated on the way through slit scattering and may therefore contribute severely to the background at extreme forward angles. The target gas was flooded inside the chamber through a 6 mm hole from one of the side ports. The gas pressure was constantly monitored and kept very low, i.e., ~0.1 m Torr for electron energies up to 100 eV and ~0.3 m Torr for higher energy electrons to minimize scattering of low-energy electrons from the gas. The chamber was continuously pumped by a 2000 l/s Turbo molecular pump to maintain a static gas condition throughout the experiment. The secondary electrons emitted were energy analyzed by the hemispherical electrostatic analyzer having inner and outer radii of 25 and 35 mm, respectively. A preacceleration voltage of 5 V was applied to the spectrometer front and exit slit to improve the collection efficiency of very-low-energy electrons (<5 eV) which can be very much affected by any stray electric or magnetic field present near the interaction region. The residual magnetic field near the interaction zone was reduced to less than 5 mGauss by setting two layers of μ metal sheets close to the inside wall of the scattering chamber. The energy analyzed electrons were finally detected by a channel electron multiplier (CEM) kept at the exit slit of the analyzer. The cone of the CEM was kept at a positive potential of 100 V, because the detection efficiency of the CEM is close to *one* for electrons having energy between 100 and 500 eV.

The detection efficiency goes down as the energy of the electron increases and hence an efficiency correction is needed to put the yield of high-energy electrons on an absolute scale. Since we are mainly interested in the below 500-eV region of the spectra, no efficiency correction to the electron spectra was required. The energy dependence of the DDCS was studied for 10 different angles between 30° and 150°. At each angle the electrons having energies between 1 and 1000 eV were detected except for 150° for which the spectrum was collected up to 500 eV. In some cases electron of energies up to 2000 eV or above were also detected.

III. COMPARISON WITH THEORY

A. Energy distributions at fixed angles

Figures 1 and 2 show the measured energy distribution of DDCS for electron emission for 6-MeV/u $C^{6+}+H_2$ collision along with the CDW-EIS predictions. We also compare the measured cross sections with the prediction of B1 calculations. The data presented shows a decrease of cross section over several orders of magnitude as the electron emission energy is increased. At low energies, approximately close to zero eV, the cross section reaches a maximum due to the contribution of the soft electron emission process. The structure at the higher energy side of the DDCS plot for 60° emission angle is due to the binary encounter electrons. The peak position (E_{BE}) of the BE peak is proportional to the impact energy and varies as $\cos^2\theta$ for a given impact energy (E_p), θ being the angle of emission [36,37],

$$E_{\mathrm{BE}} = 4t\cos^2\theta - I, \tag{1}$$

$$t = 548.4\left[\left(\frac{E_p}{M_p}\right)(\mathrm{MeV}/u)\right], \tag{2}$$

where t is the cusp energy in eV and I is the ionization potential of the 1s electron.

As can be seen from Fig. 1 and from Eq. (1), the BE peak shifts towards the lower energy side as the angle of emission is increased. It can also be noted [Figs. 1 and 2] that, as we move from 60° to 90° through 75°, the BE peak starts to merge with the low-energy continuum part of the spectrum and finally at 90° the peak completely disappears contributing to the whole energy range of the spectrum. Therefore, the binary encounter electrons have a substantial contribution, at the lower energy end of the spectrum, for forward emission angles close to 90° and at lower impact energies. The width of the BE peak is a manifestation of the Compton profile (CP) of the 1s electron in the target atom. The BE process can be regarded as a Rutherford back scattering of the target electrons when viewed from the rest frame of the projectile. For bare projectile ions, the DDCS for BE electron production is given by [36,37]

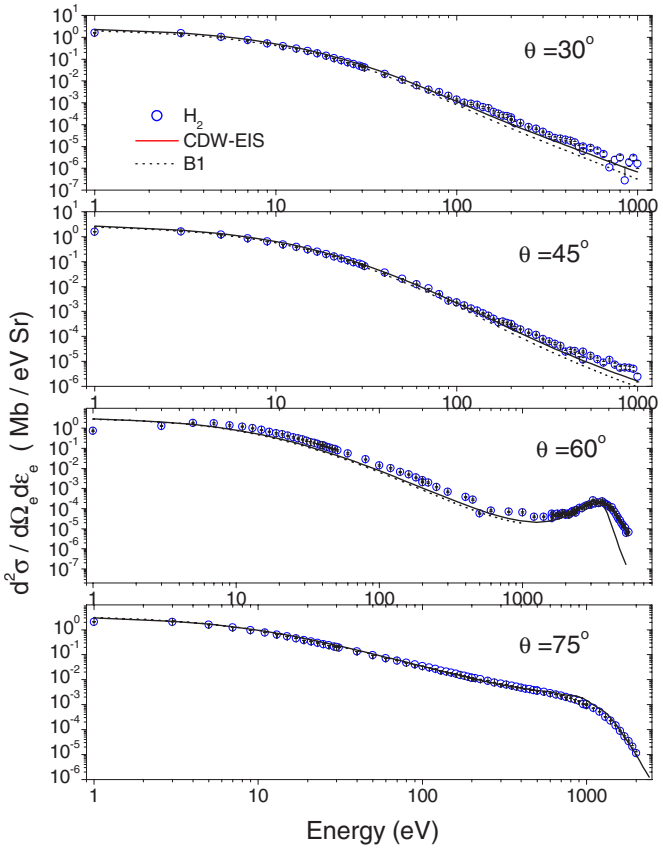

FIG. 1. (Color online) The double differential cross section of electrons for four different angles, namely 30°, 45°, 60°, and 75°. The CDW-EIS and B1 calculations are shown as solid and dotted lines, respectively.

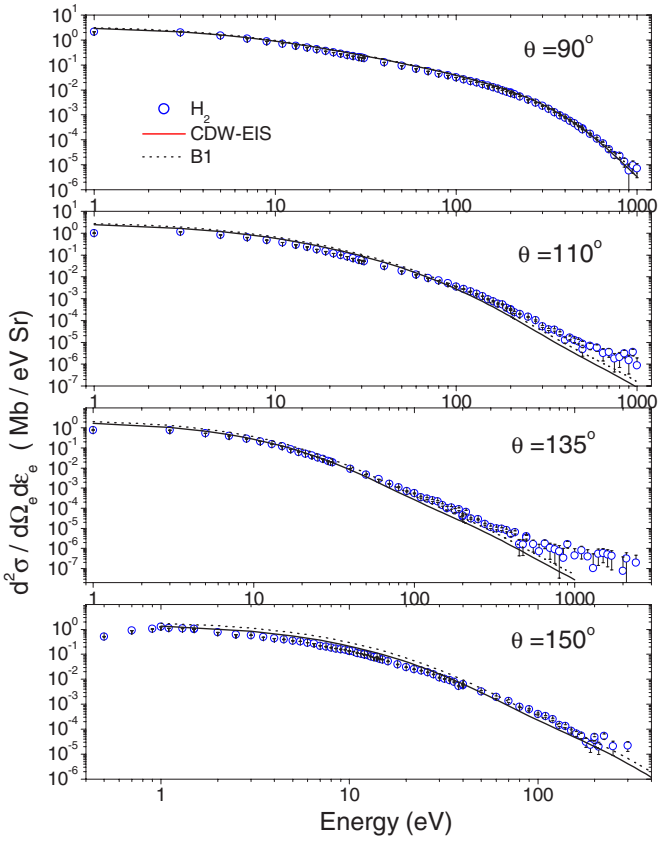

FIG. 2. (Color online) Same as in Fig. 1, except for angles 90°, 110°, 135°, and 150°.

$$\left(\frac{d^2\sigma}{d\Omega\, dE}\right)^{\text{proj}}_{\text{BE}} = \frac{J(Q)}{V_p + Q/m_e}\left(\frac{d\sigma}{d\Omega}\right)^{\text{proj}}_{\text{Rutherford}}, \tag{3}$$

where $(d\sigma/dE)^{\text{proj}}_{\text{Rutherford}}$ is the Rutherford scattering cross section in the rest frame of the projectile, and V_p is the laboratory frame projectile velocity. The argument of the CP, J, Q, the component of the target electron's momentum projected along the beam axis is given by

$$Q = \sqrt{2m_e(E_{\text{proj}} + I)} - m_e V_p, \tag{4}$$

where I is the ionization potential of the target and E_{proj} is the outgoing electron's energy in the rest frame of the projectile ion.

The effect of these BE electrons on the interference structure can be found in [25,26] at lower impact energies for 2.5-MeV/u $C^{6+}+H_2/H$ and 1.5-MeV/u $F^{9+}+H_2/H$ collision systems. All the features observed in the present spectrum are well explained by the CDW-EIS model calculations. For lower emission energies, a good agreement is found, whereas a noticeable discrepancy is observed for very-high-energy electrons at backward emission angles. The measured DDCS is found to match quite well with CDW-EIS and B1 calculations for angles close to 90°. This is due to the fact that most of the target electrons ejected close to 90° are generated from a binary collision with the projectile, hence not influenced by the receding projectile. B1 being a target-centric model, explains the result quite well. Figure 3 shows the energy distribution of the single differential cross section (SDCS) of ejected electrons along with the theoretical predictions of CDW-EIS and B1 calculations. The SDCS was derived by integrating the angular distribution of the DDCS (see below in Fig. 4). The solid line in Fig. 3 corresponds to CDW-EIS calculations using molecular distorted wave functions for the initial and final states. The dotted curve corresponds to the B1 calculations. In general an excellent agreement has been found between the experiment and the theoretical calculations.

The uncertainty in the calculation of the absolute cross section is close to ±25%, the main contribution being originated from normalization procedure adopted. The relative uncertainty in the calculation of cross section as a function of energy can be about ±10%–15% which was significant above 100 eV. The data for low-energy electrons can be associated with even higher uncertainties which could be difficult to estimate. This could be attributed to the collection efficiency of these low-energy electrons, which are easily deflected by the stray electric and magnetic fields present near the interaction zone. Again, the statistical errors for very low cross section events, where the background contribution is large, (i.e., $E_e > 500$ eV) can introduce larger uncertainties in the measured cross sections.

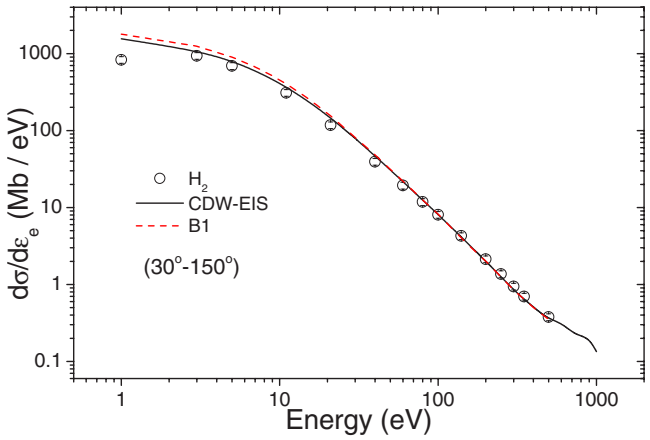

FIG. 3. (Color online) Energy distribution of single differential cross section of electrons emitted in 6-MeV/u C^{6+}+H_2 collision. The CDW-EIS and B1 calculations are shown as solid and dashed lines, respectively.

B. Angular distributions at fixed energies

Figure 4 shows the angular distributions of DDCS for H_2 at selected secondary energies along with the prediction of CDW-EIS and B1 calculations. As it can be seen from the figures, the angular distributions show a large forward-backward asymmetry due to the two-center effect in qualitative agreement with the molecular CDW-EIS calculations. This asymmetry is not reproduced by the B1 calculations, because B1 does not consider the projectile center effects. The agreement with CDW-EIS is found to be good for forward emission angles and for higher energies, whereas a noticeable discrepancy could be observed for very-low-energy electrons and at backward angles, indicating the failure of the model in explaining the backward electron emission processes. The overall agreement of CDW-EIS calculations is found to be good except for extreme backward angles where the theory underestimates the experimental results. B1 calculation underestimates the cross section at forward angles whereas it overestimates the cross sections at backward angles and the agreement is found to be good for angles close to 90°. This is due to the fact that most of the electrons ejected close to 90° are resulted from a binary collision event with the projectile, hence there is very little effect of the receding projectile ion. In case of forward angles the trajectory of the electron is highly influenced by the receding projectile, as a result a forward focusing effect happens for relatively high-energy electrons. Very low-energy electrons are assumed to be least affected by the two-center effect, because the velocities are very small compared to the velocity of the projectile ion. However, we still see a small angular asymmetry for very-low-energy electrons indicating the effect of TCE on these slow moving electrons. However, the hydrogen molecule being a two electron system, has a non-Coulombic interaction potential between the electron and the nucleus. This non-Coulombic nature of the target potential can lead to asymmetry in forward-backward electron emission [31–34].

In Fig. 5, we show the angular distribution of the SDCS of the ejected electrons along with the theoretical predictions

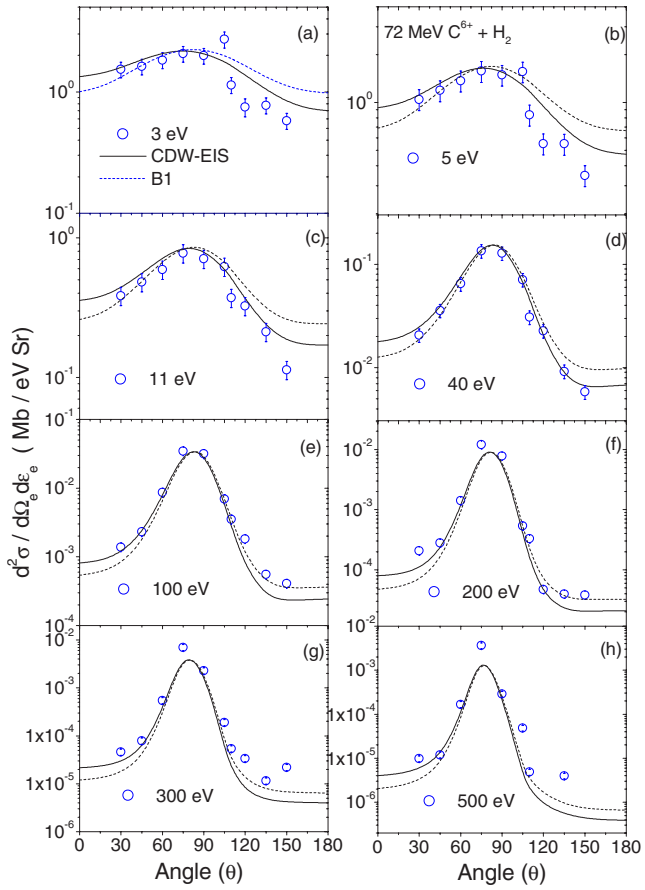

FIG. 4. (Color online) The double differential cross section of electrons for eight different emission energies, namely E_e=3, 5, 11, 40, 100, 200, 300, and 500 eV. The CDW-EIS and B1 calculations are shown as solid and dashed lines, respectively.

of CDW-EIS and B1 calculations. The solid curve in Fig. 5, corresponds to the CDW-EIS calculations using molecular distorted wave functions for the initial and final states. The dotted curve corresponds to the B1 calculations. The measured angular distribution of the SDCS shows a good agreement for forward emission angles, whereas a noticeable discrepancy can be observed at higher backward emission angles indicating the failure of the theoretical calculations.

C. Deriving interference oscillations

Since the two H atoms in molecular hydrogen are indistinguishable, their contributions to the ionization probability add coherently and an interference effect might be expected in the single ionization of H_2. Such electron emission from H_2 may be closely related to the well-known Young's two-slit experiment which provided the crucial input to the development of the quantum mechanics. Since the DDCS varies over several orders of magnitude over an energy range of 300 eV, it becomes very difficult to notice small variation of the order of 50% due to interference in the DDCS spectrum. Therefore, in order to amplify the visibility of the structure, the experimental DDCS for H_2 is divided by the corresponding calculated DDCS for H in the absence of experimental data on H as in [8,34]. The ratio $R(k,\theta)$ is plotted as a func-

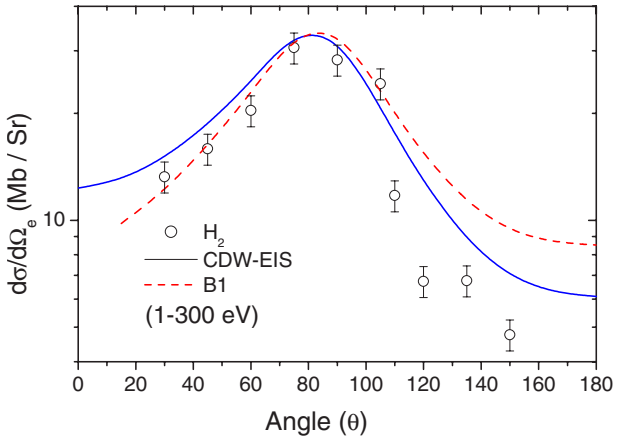

FIG. 5. (Color online) Angular distribution of single differential cross section of electrons emitted in 6-MeV/u $C^{6+}+H_2$ collision. The CDW-EIS and B1 calculations are shown as solid and dashed lines, respectively.

tion of the ejected electron velocity. In Figs. 6–8, we show such ratio spectra for several backward angles. The Figs. 6(a), 7(a), and 8(a) show the DDCS ratio for 110°, 135°, and 150°, respectively. The dotted lines (D_1) in all three panels are fitted lines through the data points which show the overall increase of the ratios as a function of electron velocity. This increasing trend of the ratios could be attributed to (i) the systematic deviation of the calculated DDCS from the actual (measured) cross sections for H. (ii) Use of different effective charge (Z_{eff}) for the calculation of DDCS, which in some way corresponds to the differences in the binding energies of the two systems. In Figs. 6(b), 7(b), and 8(b) the DDCS ratios are divided by the fitted line (D_1) to get a normalized ratio ($R_N=R/D_1$). These ratios (R_N) show oscillations around a horizontal line at 1. However, use of different values for Z_{eff}, such as 1.05, derived from the binding energy or 1.19, originated from the variational treatment of the wave function for H_2, leads to different ratios as shown in the bottom panels of Figs. 6–8. In Figs. 6(c), 7(c), and 8(c) we show the DDCS ratio for $Z_{\text{eff}}=1.05$ at 110°, 135°, and 150°, respectively, and in Figs. 6(d), 7(d), and 8(d) we show the same ratios for $Z_{\text{eff}}=1.19$. It can be noticed that the use of a higher value of Z_{eff}, yields a DDCS ratio that oscillates around a horizontal line at 1, with a slight tendency to decrease with the increase of electron velocity as opposed to the increasing behavior in the case of atomic H ($Z_{\text{eff}}=1.0$). The use of different values of Z_{eff} also changes the phase and amplitude of the oscillations. The solid curves in all the panels are the full molecular CDW-EIS calculations for H_2. It can be seen from the normalized ratios (R_N) that both the experimental and the theoretical results show the interference oscillations, although the agreement is not very good as far as the phase and the amplitude of the oscillations are concerned. The possible reason could be the limitation of the theory to reproduce the DDCS for atomic H correctly [8,34].

We also show the evidence of interference effect in the SDCS as a function of ejected electron energy. Although the calculation of SDCS involves an integration over all the

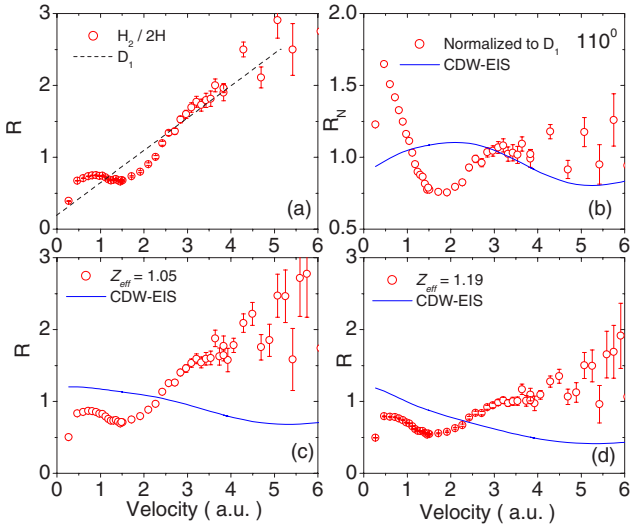

FIG. 6. (Color online) (a), (c), (d): The symbols represent the ratio $R(k,\theta)$ for different values of Z_{eff}, i.e., 1.0, 1.05, and 1.19, respectively. The dotted line D_1 in (a) is a fitted straight line. (b) Symbols represent the normalized ratio R_N for $\theta=110°$ emission angle and the solid line is a CDW-EIS calculation (see text).

emission angles, it still retains the interference information preserved. The interference structure is obtained by taking the ratio of experimental data for H_2 to the calculated values for H and then deriving the normalized ratio R_N by dividing by the fitted straight line. Figure 9 shows the normalized SDCS ratio (R_N) along with the prediction of the CDW-EIS calculations. The solid line in Fig. 9 is the prediction of the CDW-EIS calculation and the dotted line is a guide to eye. As in the case of the DDCS ratios, the SDCS ratio also shows oscillations as a function of ejected electron velocity. However, the agreement with theory is not good as far as the phases and amplitudes are concerned. This is the first time that an evidence of interference effect has been shown in the single differential cross sections of electron emission from H_2.

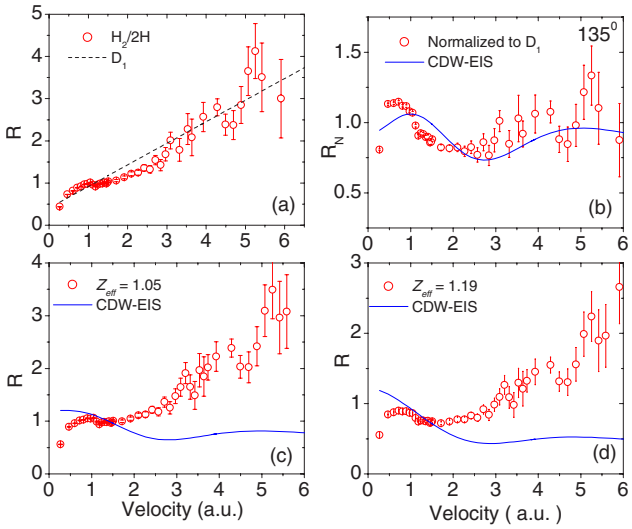

FIG. 7. (Color online) Same as in Fig. 6 except for $\theta=135°$.

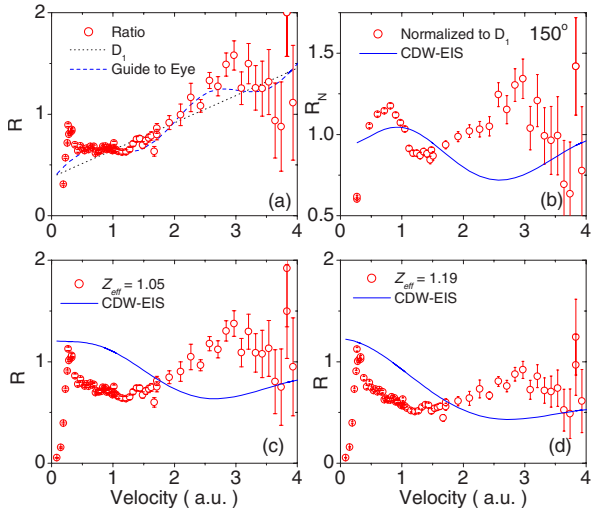

FIG. 8. (Color online) Same as in Fig. 6 except for $\theta=150°$.

D. Asymmetry parameter and interference effect

The long-range Coulomb interactions between the electron target and electron projectile in the final state influence the evolution of electron wave function and hence the angular distribution. The two-center effect as well as non-Coulomb potential for two or multielectron targets are known to cause a large forward-backward angular asymmetry [31–35], which can be seen in the large difference in the DDCS values (σ) for small forward and large backward angles. We define the quantity $\alpha(k)$ as

$$\alpha(k,\theta) = \frac{\sigma(k,\theta) - \sigma(k,\pi-\theta)}{\sigma(k,\theta) + \sigma(k,\pi-\theta)}, \tag{5}$$

where electron energy $\varepsilon_k = k^2/2$ (in a.u.) and θ is chosen to be the low forward angle, 30°. However, by expanding the $\sigma(k,\theta)$ in terms of the Legendre's polynomials, it was shown by Fainstein *et al.* [35], that, the $\alpha(k)$ would represent the angular asymmetry parameter if $\theta=0$. Since angular distributions vary slowly near 0 and π [34] the measured $\alpha(k,30°)$ approximately represents the angular asymmetry parameter.

The derived values of $\alpha(k)$, [i.e., $\alpha(k,30°)$] show a smooth monotonically increasing trend as a function of electron velocity, for an atomic target such as He (Fig. 10). This behavior is expected based on the two-center electron emission process which is qualitatively well represented by the CDW-EIS model [35]. On the contrary, for C^{6+} colliding with H_2, the asymmetry parameter shows an oscillatory structure superimposed on a smoothly varying function. This difference in the behavior between an atomic and molecular target at such high-energy collision was unexpected based on the independent electron approximation and two-center effect alone.

To understand this effect we use the molecular CDW-EIS calculation [9]. The main feature of this model is to represent the initial bound state of the active electron by a two-center molecular wave function. Within the impact parameter approximation, the transition amplitude reduces to a coherent sum of atomic transition amplitudes corresponding to individual molecular centers. This model, however, automatically reproduces the Young-type interference effect in the electron emission from H_2 and its dependence on the emission angle such that the frequency of oscillation is higher for backward angles compared to the complementary forward ones. This difference in the frequency, for forward and backward angles, causes the oscillatory structure in the $\alpha(k)$. It can be seen (Fig. 10) that molecular CDW-EIS predicts the oscillation in the α values between 1 and 5 a.u. On the contrary, the atomic-type CDW-EIS calculation [2] based on independent electron approximation, i.e., using an effective atomic number ($Z_{\text{eff}}=1.19$) for atomic H does not produce (dashed-dotted line in Fig. 10) any oscillation and behaves like a single center target such as the He atom. This again implies that the interference process built-in molecular CDW-EIS model using molecular wave function gives rise to the oscillations in the asymmetry parameter for H_2.

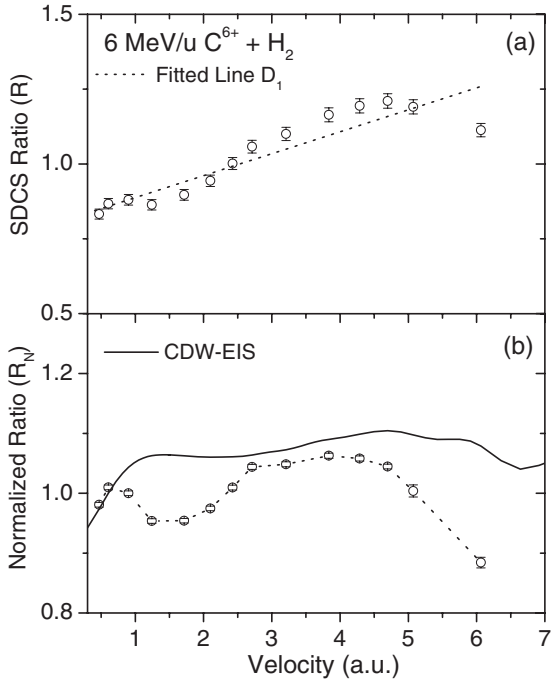

FIG. 9. (a) The SDCS ($d\sigma/d\epsilon_e$) ratio for the electron emission in collisions of 6-MeV/u C^{6+} with H_2. The dotted line is a straight line fit to the data. (b) The normalized ratio obtained by dividing the ratio by the fitted line D_1. Solid line is the CDW-EIS calculations, and dotted line is to guide the eyes.

However, for completeness and to get a deeper insight into the problem, we have recently developed a model [28] which we apply here by discussing more details about it. Following Cohen and Fano [3], Stolterfoht *et al.* [7] have used the following expression for the DDCS for low-energy electron emission from H_2 (under dipole approximation [38]):

$$\sigma_{H_2}(k,\theta_i) = A_i(k)\left(1 + \frac{\sin(kcd)}{kcd}\right), \tag{6}$$

where d is the internuclear separation (1.4 a.u.) and c is an adjustable frequency parameter. If the momentum transfer is

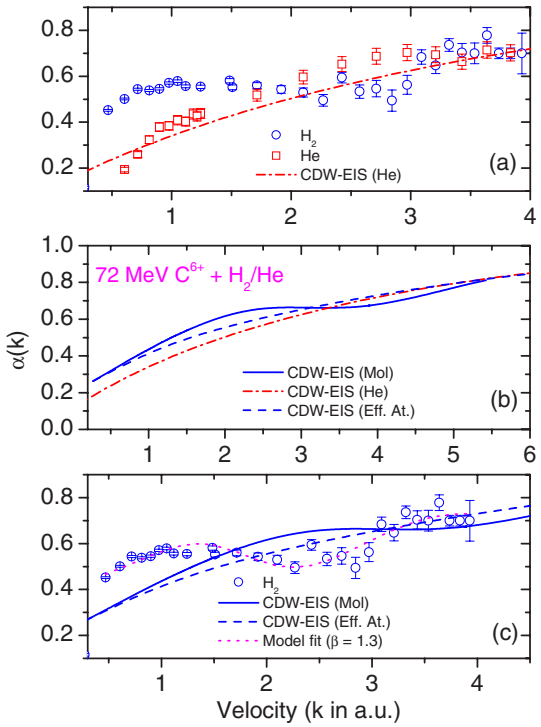

FIG. 10. (Color online) The asymmetry parameter: symbols represent the experimental data for collision of 6-MeV/u C^{6+} with H_2 (open circles) and He (open squares). Solid line represents the molecular CDW-EIS calculation for H_2; dashed line is the effective atomic CDW-EIS calculation (Z_{eff}=1.19) for H_2; dashed-dotted line corresponds to the atomic CDW-EIS calculation for He and the dotted line is the model fit to the H_2 data (see the text below) with $|\beta|$=1.3.

completely neglected (like in the dipole approximation) the parameter $c=1$. If only the transverse momentum transfer is neglected it has been shown in [10] using a peaking approximation that $c=\cos\theta$. This simple result predicts therefore that the frequency is the same for two complementary angles θ_1 and $\theta_2=\pi-\theta_1$. Experimental observations by Stolterfoht *et al.* [19] and Misra *et al.* [8], however, reveal that the oscillations at backward angles have higher frequency. Theoretical calculations without any assumption about the momentum transfer [12,14], reproduce indeed this asymmetry although the predicted values at large emission angles are lower than the experimental results. Therefore, we define the DDCS in terms of a frequency which has a still unknown θ dependence,

$$\sigma_{H_2}(k,\theta_i) = A_i(k)\left(1+\frac{\sin\{k[\Theta(\theta_i)]d\}}{\{k[\Theta(\theta_i)]d\}}\right). \tag{7}$$

Let us define, $a_i=\Theta(\theta_i)$ and $\beta=a_j/a_i$ which is essentially the ratio of the frequency observed for θ_i and θ_j. A generalized asymmetry parameter now can be defined, as in Eq. (5),

$$\alpha(k) = \frac{\sigma(k,a_i)-\sigma(k,a_j)}{\sigma(k,a_i)+\sigma(k,a_j)}. \tag{8}$$

Using Eq. (5) and using $\beta=a_j/a_i$ (and setting $a_i=a$) one gets

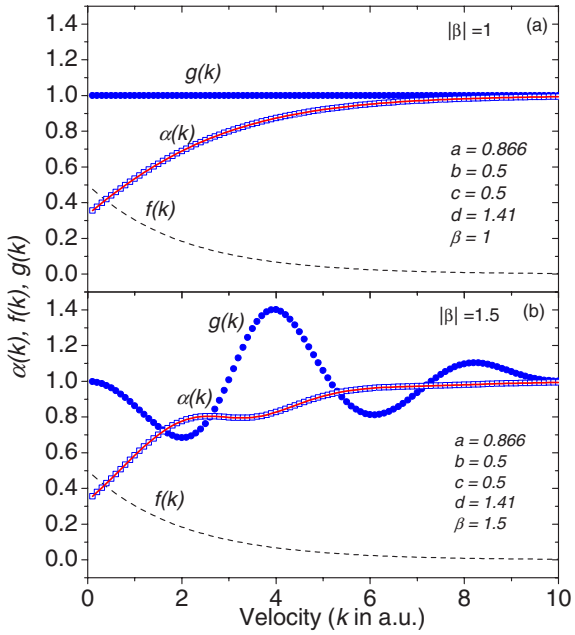

FIG. 11. (Color online) The calculated values [Eqs. (11)–(13)] of $\alpha(k)$, $f(k)$, and $g(k)$ for $|\beta|=1$ (a) and $|\beta|=1.5$ (b). The parameters, a [=cos(θ)], b, c, d (=1.41 a.u., equilibrium bond length of H_2), and β in (a) and (b) are defined in Eqs. (12) and (13).

$$\alpha(k) = \frac{\beta kda(A_i-A_j)+(A_i\beta\sin[kda]-A_j\sin[\beta kda])}{\beta kda(A_i+A_j)+(A_i\beta\sin[kda]+A_j\sin[\beta kda])}. \tag{9}$$

If $\beta=-1$, i.e. if $\Theta(\theta_i)=\cos\theta_i$,

$$\alpha(k) = \frac{A_i(k)-A_j(k)}{A_i(k)+A_j(k)}, \tag{10}$$

which is free from any oscillatory behavior and increases monotonically with k [shown in Fig. 11(a)]. Now if $\beta\neq-1$,

$$\alpha(k) = \frac{1-g(k)f(k)}{1+g(k)f(k)}, \tag{11}$$

where

$$f(k) = A_j(k)/A_i(k) = be^{-ck} \tag{12}$$

and

$$g(k) = \left(\frac{1+\dfrac{\sin[\beta kda]}{\beta kda}}{1+\dfrac{\sin[kda]}{kda}}\right). \tag{13}$$

The function $f(k)$ is proportional to the incoherent (nonoscillatory) part of the DDCS. It is a smoothly decreasing function of k which resembles essentially the DDCS for any atomic target and was chosen to be be^{-ck} (b and c are fitting parameters). For $|\beta|=1$, $g(k)=1$, as shown in Fig. 11(a). If $|\beta|\neq1$ then $g(k)$ becomes an oscillatory function of k [see Eq. (13) and Fig. 11(b)] and therefore the resultant $\alpha(k)$ shows an oscillation. One such example is given in Fig.

11(b) for $|\beta|=1.5$. The difference in the oscillation frequencies, for two complementary angles, gives rise to the oscillatory structure in $\alpha(k)$. The data in Fig. 10(c) is fitted using this model (dashed-dotted line) and the main fitting parameter $|\beta|=1.3$.

A good fitting of the oscillatory structure in Fig. 10 to the above model (dashed-dotted line) indicates that the simple expression of interference-influenced DDCS using a Cohen-Fano-type function [3] can generally explain the phenomenon. It may also be noted that the CDW-EIS model [solid line in Fig. 10(c)] calculation also provides a qualitative agreement although with a lower frequency of oscillation than the fitted line. This difference is not surprising since the dashed-dotted line is only a model fit to the data, whereas the solid line is a result obtained from an *ab initio* theory using molecular wave function. Given the complexity of the processes involved and the perturbative nature of the calculation the qualitative agreement obtained by the CDW-EIS approach is quite reasonable. However, it is obvious from the analysis in terms of these models that the interference plays a major role in the asymmetry parameter such that this parameter itself will be a sensitive tool to explore the interference effect. In addition, a deviation of $|\beta|$ from 1.0 (i.e., about 1.3) implies that for backward angle the frequency of oscillation cannot be governed by only the longitudinal component of the momentum transfer, i.e., the simple $\cos\theta$ dependence which seems to explain the forward angle data only. One may note here that the present value of β, which is obtained using $30°-150°$ combination, is lower compared to our earlier observation [28] for which the complementary angles were chosen to be lower and higher extreme angles, such as, 20° and 160°. This means the asymmetry in the frequency reduces for the complementary angles closer to 90° giving a smaller value of β (i.e., close to 1.0). This observation has been seen to be consistent with our other data sets taken at different energies as well as for different complementary angles such as $45°-135°$, etc. In addition, this provides an important tool to study the interference phenomena for molecular target without making a comparison with the similar data with corresponding atomic target. Therefore, this technique can be used, in principle, for other diatomic targets for which getting the experimental or theoretical data for the corresponding atomic target is difficult to get. Very recently it has been shown [39] that ejected electron angular distribution in e-2e ionization of H_2 gets modified due to the interference effect, in agreement with our recent observation [28].

IV. CONCLUSIONS

We have demonstrated that the measurements of the electron DDCS in case of the molecular hydrogen provide crucial information regarding the two-center effect and also on the interference effect. The overall agreement of CDW-EIS calculations is found to be good except for extreme backward angles where the theory underestimates the experimental results. The B1 calculation underestimates the cross sections at forward angles whereas it overestimates the cross sections at backward angles. However, the agreement is found to be good for angles close to 90°. A technique of extracting interference effect has been proposed by invoking the effect of interference on the forward-backward asymmetry parameter, which simplifies the experimental procedure. The present technique may be unique for the study of interference effect in case of diatomic molecules such as N_2, O_2, etc., since for these multielectronic atoms (e.g., O, N, etc.) the experimental and even theoretical investigations are challenging tasks. In addition, it is demonstrated that the asymmetry in electron emission is influenced by this mechanism, i.e., the interference effect other than the known mechanisms. The single differential cross sections, i.e., $d\sigma/d\Omega_e$ and $d\sigma/d\epsilon_e$ have also been derived, and the evidence of interference effect has been observed in the single differential cross section, $d\sigma/d\varepsilon_e$

[1] D. S. F. Crothers and J. F. McCann, J. Phys. B **16**, 3229 (1983).
[2] L. Gulyás, P. D. Fainstein, and A. Salin, J. Phys. B **28**, 245 (1995).
[3] H. D. Cohen and U. Fano, Phys. Rev. **150**, 30 (1966).
[4] M. Walter and J. S. Briggs, J. Phys. B **32**, 2487 (1999).
[5] T. F. Tuan and E. Gerjuoy, Phys. Rev. **117**, 756 (1960).
[6] S. E. Corchs, R. D. Rivarola, J. H. Mcguire, and Y. D. Wang, Phys. Scr. **50**, 469 (1994).
[7] N. Stolterfoht, B. Sulik, V. Hoffmann, B. Skogvall, J.-Y. Chesnel, J. Rangama, F. Frémont, D. Hennecart, A. Cassimi, X. Husson, A. L. Landers, J. A. Tanis, M. E. Galassi, and R. D. Rivarola, Phys. Rev. Lett. **87**, 023201 (2001).
[8] Deepankar Misra, Umesh Kadhane, Y. P. Singh, L. C. Tribedi, P. D. Fainstein, and P. Richard, Phys. Rev. Lett. **92**, 153201 (2004).
[9] M. E. Galassi, R. D. Rivarola, P. D. Fainstein, and N. Stolterfoht, Phys. Rev. A **66**, 052705 (2002).
[10] L. Nagy, L. Kocbach, K. Póra, and J. P. Hansen, J. Phys. B **35**, L453 (2002).
[11] G. Laurent, P. D. Fainstein, M. E. Galassi. R. D. Rivarola, L. Adoui, and A. Cassimi, J. Phys. B **35**, L495 (2002).
[12] L. Sarkadi, J. Phys. B **36**, 2153 (2003).
[13] C. R. Stia, O. A. Fojón, P. F. Weck, J. Hanssen, and R. D. Rivarola, J. Phys. B **36**, L264 (2002).
[14] M. E. Galassi, R. D. Rivarola, and P. D. Fainstein, Phys. Rev. A **70**, 032721 (2004).
[15] K. Póra and L. Nagy, Nucl. Instrum. Methods Phys. Res. B **233**, 293 (2005).
[16] R. Della Picca, P. D. Fainstein, M. L. Martiarena, and A. Dubois, J. Phys. B **39**, 473 (2006).
[17] A. J. Murray, M. J. Hussey, J. Gao, and D. H. Madison, J. Phys. B **39**, 3945 (2006).
[18] X.-J. Liu, N. A. Cherepkov, S. K. Semenov, V. Kimberg, F. Gel'mukhanov, G. Prümper, T. Lischke, T. Tanaka, M. Hoshino, H. Tanaka, and K. Ueda, J. Phys. B **39**, 4801 (2006).

[19] N. Stolterfoht, B. Sulik, L. Gulyás, B. Skogvall, J.-Y. Chesnel, F. Frémont, D. Hennecart, A. Cassimi, L. Adoui, S. Hossain, and J. A. Tanis, Phys. Rev. A **67**, 030702(R) (2003).
[20] N. Stolterfoht, B. Sulik, B. Skogvall, J.-Y. Chesnel, F. Frémont, D. Hennecart, A. Cassimi, L. Adoui, S. Hossain, and J. A. Tanis, Phys. Rev. A **69**, 012701 (2004).
[21] A. L. Landers, E. Wells, T. Osipov, K. D. Carnes, A. S. Alnaser, J. A. Tanis, J. H. McGuire, I. Ben-Itzhak, and C. L. Cocke, Phys. Rev. A **70**, 042702 (2004).
[22] S. Hossain, A. L. Landers, N. Stolterfoht, and J. A. Tanis, Phys. Rev. A **72**, 010701(R) (2005).
[23] K. Støchkel, O. Eidem, H. Cederquist, H. Zettergren, P. Reinhed, R. Schuch, C. L. Cocke, S. B. Levin, V. N. Ostrovsky, A. Källberg, A. Simonsson, J. Jensen, and H. T. Schmidt, Phys. Rev. A **72**, 050703(R) (2005).
[24] F. Frémont, A. Hajaji, A. Naja, C. Leclercq, J. Soret, J. A. Tanis, B. Sulik, and J.-Y. Chesnel, Phys. Rev. A **72**, 050704(R) (2005).
[25] Deepankar Misra, U. Kadhane, Y. P. Singh, L. C. Tribedi, P. D. Fainstein, and P. Richard, Phys. Rev. Lett. **95**, 079302 (2005).
[26] J. A. Tanis, S. Hossain, B. Sulik, and N. Stolterfoht, Phys. Rev. Lett. **95**, 079301 (2005).
[27] J. A. Tanis, J.-Y. Chesnel, B. Sulik, B. Skogvall, P. Sobocinski, A. Cassimi, J.-P. Grandin, L. Adoui, D. Hennecart, and N. Stolterfoht, Phys. Rev. A **74**, 022707 (2006).
[28] Deepankar Misra, A. Kelkar, U. Kadhane, Ajay Kumar, Lokesh C. Tribedi, and P. D. Fainstein, Phys. Rev. A **74**, 060701(R) (2006).
[29] D. Misra, Ajay Kumar, U. R. Kadhane, P. D. Fainstein, and L. C. Tribedi, Radiat. Phys. Chem. **75**, 1723 (2006).
[30] Daniel Rolles, Markus Braune, Slobodan Cvejanović, Oliver Geßner, Rainer Hentges, Sanja Korica, Burkhard Langer, Toralf Lischke, Georg Prümper, Axel Reinköster, Jens Viefhaus, Björn Zimmermann, Vincent McKoy, and Uwe Becker, Nature (London) **437**, 711 (2005).
[31] N. Stolterfoht, H. Platten, G. Schiwietz, D. Schneider, L. Gulyás, P. D. Fainstein, and A. Salin, Phys. Rev. A **52**, 3796 (1995).
[32] J. O. P. Pedersen, P. Hvelplund, A. Petersen, and P. D. Fainstein, J. Phys. B **24**, 4001 (1991).
[33] S. Suárez, C. Garibotti, W. Meckbach, and G. Bernardi, Phys. Rev. Lett. **70**, 418 (1993).
[34] Lokesh C. Tribedi, P. Richards, W. DeHaven, L. Gulyás, M. W. Gealy, and M. E. Rudd, J. Phys. B **31**, L369 (1998).
[35] P. D. Fainstein, L. Gulyás, F. Martin, and A. Salin, Phys. Rev. A **53**, 3243 (1996).
[36] N. Stolterfoht, D. Schneider, R. Burch, H. Wieman, and J. S. Risley, Phys. Rev. Lett. **33**, 59 (1974).
[37] D. H. Lee, P. Richard, T. J. M. Zouros, J. M. Sanders, J. L. Shinpaugh, and H. Hidmi, Phys. Rev. A **41**, 4816 (1990).
[38] H. A. Bethe, Ann. Phys. **5**, 325 (1930).
[39] D. S. Milne-Brownlie, M. Foster, Junfang Gao, B. Lohmann, and D. H. Madison, Phys. Rev. Lett. **96**, 233201 (2006).